Celal Bayar University Journal of Science

Effects of Thin Film Morphology of Polymer Hole Transfer Material on Photovoltaic Performance of Perovskite Solar Cells

Oğuz Çiçek[1] (iD), Burak Gültekin[1*] (iD)

Ege University Solar Energy Institute, 35100 Bornova İzmir, Türkiye
*burak.gultekin@ege.edu.tr
* Orcid: 0000-0002-8804-7844

Abstract

In the present study, the effects of chain length variation of Poly(3-hexyl) thiophene polymer, which is one of the appropriate alternatives of Spiro-O-MeTAD used as a hole transfer layer (HTL) in perovskite-based solar cells (PSC), on thin-film morphology and device performance were investigated. Furthermore, nanowires of long (UZ) and short-chain (KZ) P3HT were obtained in the solution phase and then comparative photovoltaic performance analyses were carried out by fabricating PSC devices. As a result, it was determined that the morphological changes resulting from the polymer chain length directly affect the charge transfer between the active layer and HTL. KZ-P3HT presented better performance than both standard P3HT (5.99) and UZ-P3HT (2.68) polymers with a power conversion efficiency (PCE) of 7.74%. It was demonstrated that the main reason for this is that the fringed structure, detected by AFM images, increases the contact ratio at the perovskite/HTM interface. In addition, thanks to the morphological improvements in nano-wire studies, it was observed that the photovoltaic performance of the PSC device containing UZ-P3HT increased by 5.51%. Contrary to UZ-P3HT, it was determined that after the conversion of KZ-P3HT to the nanowire, the fringed structure on the surface disappeared and therefore the efficiency decreased to 5.81%.

1. Introduction

Solar energy is one of the most important and promising types of renewable energy sources. Today, a power conversion efficiency (PCE) of 26.1% has been achieved with silicon-based solar cells that convert solar energy into electrical energy and dominate the market commercially [1]. New photovoltaic (PV) technologies need to be developed because of the high energy consumption during the production of silicon-based solar cells and their rigid structure, making them unsuitable for some energy applications [2],[3]. Perovskite solar cells, which are among the photovoltaic technologies defined as third generation or emerging technologies, have reached an energy conversion efficiency of 25.5% with the structural development they have demonstrated in recent years [1].

Planar multi-junction perovskite solar cells (PSC) have great potential in the production of high-efficiency, low-cost and flexible photovoltaic devices [4]. Planar PSCs have a perovskite active layer placed between the hole and electron transfer layers. Interlayers that provide

charge transfer play an important role in charge collection, extraction and transport. Small molecules and polymeric structures that can be used at these interfaces offer advantages such as being able to prepare solutions at low temperatures, thanks to their adjustable chemical and electronic structures [5]. In addition, high-performance PSCs have obvious advantages over other devices with their electrical and optical properties such as wide carrier diffusion length, direct Bandgap, high absorption coefficient in the visible near-infrared region, and high charge carrier mobility. PSCs can be produced with n-i-p or p-i-n (inverted) device structures. Vapor phase deposition techniques, vapor assisted solution treatment and annealing procedures have made significant progress in the improvement of the perovskite film [3], [6], [7]. High-efficiency PSCs use mesoporous or compact metal oxides as the electron conduction layer (ETL) under the perovskite layer. Among these materials, semiconductor oxides such as TiO_2 and SnO_2 are the most well-known and used ones in PSC devices [8], [9]. The stable structure and sufficient electron mobility of TiO_2 provide advantages for PSC applications [10]–[12]. On the other hand, the

hole transfer layer (HTL) acts as a barrier, preventing electron transfer between the anode and the perovskite layer. It is an effective method to increase the efficiency of the hole transport process, improve the V_{OC} value, and to prevent possible degradation at the perovskite-contact interface [13]. By using HTMs with high hole mobility, high efficiencies can be achieved with compatible ionization potentials (or energy levels), high thermal stability, and resistance to external degradation factors (such as oxygen and moisture) [14]–[16]. Spiro-O-MeTAD is the most widely used molecular structure in the literature as HTM. Thanks to its three-dimensional structure, it covers the perovskite surface very well. In addition, it fills the cracks on the surface and reduces the load trapping at the interfaces [17]. Despite its important advantages, The high cost due to the multi-step and complexity of the synthesis procedure of Spiro-O-MeTAD is still an important issue to be overcome. In addition, the necessity of doping to increase its low hole mobility and low conductivity complicates the device manufacturing process. Therefore, the HTM layer becomes an important problem for the commercialization of PSC devices [18]. In the doping process of the HTM layer, lithium bis(trifluoromethane sulfonyl)imide (Li-TFSI) increases the majority of charge carriers by oxidation and thereby increases the conductivity of the HTM layer. In addition, tert-butyl pyridine (TBP) regulates the morphology by reorganizing Spiro-O-MeTAD molecules oxidized with Li-TFSI and helps to adjust the energy levels with its basic character [17]. Despite the record yields achieved by doping, using additives is a factor that increases the difficulty level of cell production and the total cost. From these points of view, developing new types of HTMs, which can be synthesized easily and do not need to be doped, have a relatively low cost, high operating stability is an important subject for studying.

In the literature, there are studies on the use of semiconductor small molecules or polymers, which are already tried in many opto-electronic applications, without using chemical doping. In those investigations, the solvent engineering method was used to adjust the morphological properties of the HTM layer for efficient charge transfer [19]. The regioregular isomer of poly(3-hexyl)thiophene (P3HT) has been extensively used as a standard in the active layer in organic solar cells (OSC). In addition to this, P3HT has been involved in the PSC applications as the HTM layer. It is well known in the literature that the chain length of P3HT has significant effects on film morphology [20]–[22]. It has been reported that a smooth morphology is obtained with chain lengths over 85,000D used in the active layer in OSC applications, while the morphology is impaired and the charge transport decreases with shorter chain lengths [20], [23]. For PSC applications where P3HT is used as HTM, studies on PCE changes depending on chain length have been carried out, and it has been

reported that higher yields are achieved with an increase in chain length [24]. On the other hand, to increase the charge carrying capacity of P3HT, which has mobility of 0.1 $cm^2V^{-1}s^{-1}$, and to extend the absorption band, converting it into a nanowire is a method used in the literature. In OSC applications with nanowire P3HTs, which were grown by optimizing solvent polarity, temperature and time parameters, a mobility of 1.44 $m^2V^{-1}s^{-1}$ and a PCE of 2.40% were achieved [24].

In the presented article, two fractions of P3HT with short (KZ) and long-chain (UZ) lengths and nanowire structures of these fractions were used as HTM in PSC and PV performance comparisons of these polymers were carried out. In addition, both Spiro-O-MeTAD and mixed P3HT were used as standard. Furthermore, morphological properties of both perovskite and HTM thin film have been investigated by SEM and AFM analyses in order to express the photovoltaic performance changes of PSC devices.

2. Materials and Methods
2.1 Materials

Glasses with fluorine-doped tin oxide (FTO) as the conductive oxide layer were supplied from Pilkington company in 2.5 cm x 2.5 cm dimensions. The surface resistivity levels are 13 Ω/sq and the FTO layer thickness is 450nm. The materials used for the triple cation Perovskite active layer solution were obtained from different companies: lead iodide (PbI_2) from TCI, methyl ammonium bromide ($MABr_2$) from Lumtec, cesium iodide (CsI) from Acros, lead bromide ($PbBr_2$) from Aldrich tan and formamidinium iodide (FAI) were purchased from Lumtec.

The starting material, titanium isopropoxy ($TiOPr_4$) used for the compact titanium dioxide (TiO_2) layer solution as the electron transfer material was obtained from Aldrich company. Hollow carrier materials, Spiro-O-MeTAD and poly(3-hexyl) thiophene (P3HT) were obtained from Lumtec. In addition, Lithium bis(trifluoromethanesulfonyl)imide (Li-TFSI) was purchased from Lumtec and 4-t-butyl pyridine (4-TBP) was purchased from Aldrich companies. Contact material silver, locally sourced. Zinc (Zn) powder and hydrochloric acid (HCl) used for etching the FTO from the glass substrate surface were obtained from VWR companies. Solvents used in the experiments were purchased from different companies: hexane from Fisher, isopropyl alcohol (IPA), acetone and chlorobenzene from Sigma-Aldrich, acetonitrile from Riedel, dimethyl sulfoxide (DMSO) from Merck, and dimethylformamide (DMF) from Sigma. Pure water, on the other hand, was used from the GFL brand ultrapure water device within the institute.

2.2 Device preparation

FTO glasses were used as both the substrate and the anode of the solar cell. In accordance with the geometry of the solar cell, one side of the FTO (~1.2 cm wide) was etched. The process was carried out by applying zinc (Zn) powder and 4 M HCl (hydrochloric) acid solution to the FTO. Afterwards, purified water, acetone, and isopropyl alcohol (IPA) were used for cleaning, respectively. The glasses were placed on the glass cleaning rack and sonicated in an ultrasonic bath for 5 minutes in those solvents. In the final stage of the cleaning process, substrates were dried with a nitrogen gun and exposed to oxygen plasma for 7 minutes to get rid of organic impurities on the surface and activate the surface. Compact TiO_2 was used as the electron transfer layer. The preparation of compact TiO_2 solution was carried out in two steps. In the first step, mixtures of IPA (2.53 ml)-HCl acid (35 μl) and IPA (2.53 ml)-TiOPr4 (0.369 ml) were placed in two separate vials. A compact TiO_2 solution was prepared by adding the solution containing TiOPr4 to the other solution. The substrates, whose surfaces were cleaned of organic residues with oxygen plasma, were coated with compact TiO_2. The coating process was carried out in the spin coater at 2000 rpm in 20 seconds. Then this layer was sintered at 460 ºC for 1 hour.

Triple cation perovskite was used as the active layer. During the preparation of triple cation Perovskite (Cs0.15 FA0.81 MA0.14 PbI2.53 Br0.45) solution, PbI2 (470 mg), PbBr2 (66 mg), MABr2 (18.81 mg), FAI (167 mg) and CsI (15 mg) was mixed stoichiometrically into 1 mL of DMF:DMSO in a 4:1 ratio [2]. During the coating process of the perovskite active layer, 80 μL of the mixture was used and the process was carried out at 2000-4000 rpm (10-20 seconds). Washing was performed with 100 μL of chlorobenzene in the last 10 seconds of the coating process. Finally, in order for the perovskite active layer to crystallize and get rid of chlorobenzene (1 hour at 100 ºC), annealing was applied. Spiro-O-MeTAD and P3HT were used as hole transfer layer for standard devices. The P3HT polymer was used both as purchased without any pre-treatment and after it was separated into two fractions as high molecular weight and low molecular weight by preparative high-performance liquid chromatography (P-HPLC) system.

A chlorobenzene solution of Spiro-O-MeTAD (76 mg/ml) was prepared for the films obtained with the spin coating system. 16 μL of 4-TBP and 30 μL of Li-TFSI were added to the mixture prepared for doping the HTM layer. During the Spiro-O-MeTAD coating, 60 μL of the solution was used for each device and the coating process was carried out with a program consisting of 20 s rotation at 4000 rpm. For the coating of P3HT HTMs, solutions of 10 mg/mL in chlorobenzene were prepared without adding any additives. In these mixtures, 80 μL was taken for each film, and the coating process was

carried out at a rotational speed of 2000 rpm for 20 s of rotation. P3HT coated films were then dried (5 min at 80 ºC) [25]. After the HTM layers were coated, silver (Ag) contacts were coated on the FTO/compact TiO2/ABX3/HTM structure. By using suitable masks, evaporation process was carried out with a thermal evaporation system in a pressure environment of ~ 4x10-6 mbar so that contact can be made from both FTO and HTM. Ag contact thickness was determined as 100 nm. Another hole transfer layer application is the P3HT nanowire application. P3HT nanowires were formed by adding KZ and UZ-P3HT materials obtained from P-HPLC to 10 mg/ml chlorobenzene: hexane (ratio: 6:4) solution and then keeping those solutions at room temperature for 1 h without stirring. The resulting solutions were filmed with the same coating and drying process as P3HT mixtures [26].

2.3 Analysis Methods
2.3.1 Characterization of Materials

X-ray diffraction (XRD) technique (Rigaku Ultima IV multi-mode XRD, $Cu_{K\alpha}$,1.54 Å) was used for the structural characterization of the triple cation perovskite active layer. All XRD analyses were performed using the CBO (cross-beam-optics) multilayer mirror system as a monochromator, with tube voltage and current of 40 V and 40 mA, respectively, from 10° to 60° (2Θ) with 0.5° scanning range and a scanning speed of 2°/min. In addition, atomic force microscope (AFM, Park AFM NX20) and scanning electron microscope (SEM, Zeiss VP 300) images were used for the surface analyses of the obtained perovskite and HTM layers. AFM analyses were performed using silicon nitride (Si_3N_4) tips smaller than 7 nm in "tapping-mode".
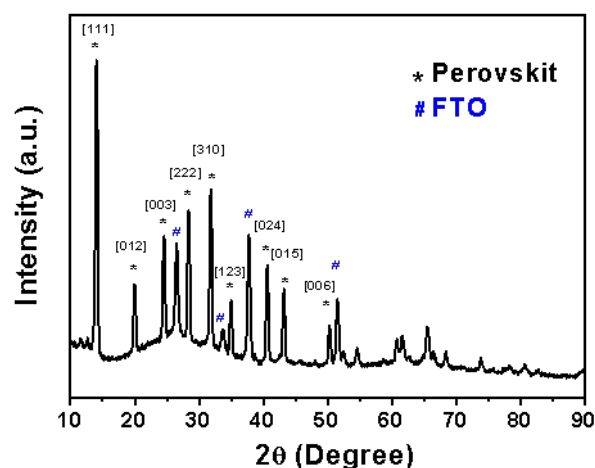
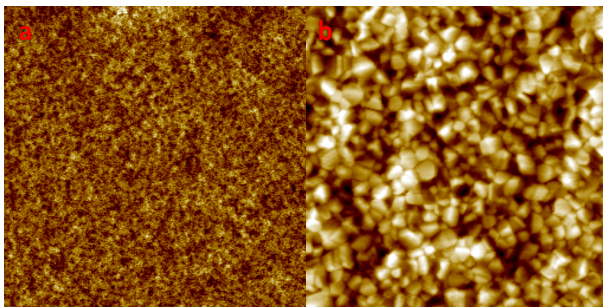**Figure 1.** XRD pattern of triple cation perovskite coated on FTO glass.

Furthermore, SEM analyses were carried out at an accelerating voltage of 3 kV and magnification of 25kX and 100kX.

2.3.2 Photovoltaic (PV) Performance Analyses

The PV performances of prepared PSC devices were determined by extracting the current-voltage curves (scanning speed: 0.1 Vs^{-1}) under AM 1.5 standard radiation in an inert atmosphere, and the incident photon to current conversion efficiency (IPCE) analyses was taken under monochromatic light (scanning range: 1 nm).

3. Results and Discussion

The perovskite active layer was prepared as reported in previous studies [2]. The pattern of the XRD analysis performed for the structural analysis of the perovskite layer is shown in Figure 1. The characteristic XRD peaks of triple cation perovskite were observed at ~14º, 24º, 31º and 43º. These peaks belong to structures (111), (003), (123), and (015), respectively, and are in good agreement with the literature [27]. However, a PbI$_2$ peak around 12º was observed, albeit in a small amount. In addition, AFM and SEM analyses were performed to examine the morphological properties of the prepared perovskite layers (Figure 2-3).


Figure 2. (a) 50µm and (b) 5µm AFM images of triple cation perovskite thin film.

In perovskite crystals, the grain boundaries of the crystal particles are act as trap states for charges [28]. Therefore, small particle sizes or wide intersection distances cause ascending of charge trap levels and descending in current density in device applications. It has been reported in many publications that annealing of perovskite thin films at 100 °C for 1 hour provides optimized crystal structure [29]. In both SEM and AFM images, it is observed that the size of the crystal domains is close to each other, indicating a homogeneous crystal growth on the compact TiO$_2$ layer. Furthermore, as can be seen from the 50µm*50µm AFM image in Figure 2(a), the distance between the deepest point and the highest point on the film is 100 nm, and this roughness is homogeneously distributed on the surface. A similar situation exists in the 25k X SEM image in Figure 3(a). The sizes of the crystal particles and the distances between the particles show a regular distribution throughout the thin film and support the AFM image. However, crystal defects marked with red rings are observed, especially in the 100.00KX SEM
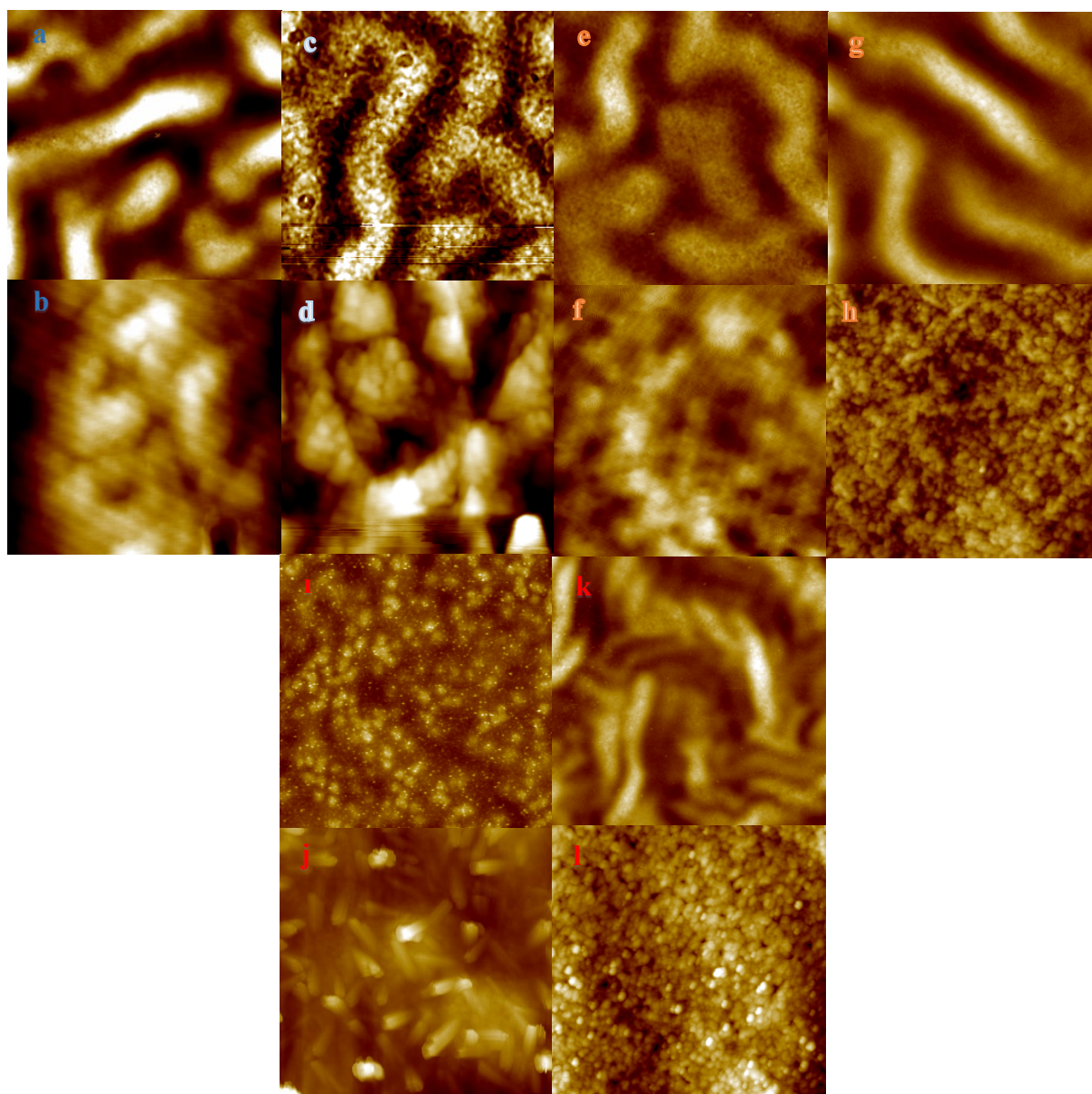
image in Figure 3(b). These defects would affect the charge transfer between the active layer and the HTM layer by increasing the trap states in the same way as grain boundaries. On the other hand, from the 2µm*2µm image obtained by the AFM technique, which allows us to obtain a three-dimensional (3D) image of the surface, it is seen that the crystals do not have a flat surface, unlike the two-dimensional (2D) SEM image. It has been determined that perovskite crystals are located on the film as mounds with sharp or pointed peaks. In contrast to the SEM image, the presence of smaller crystals was detected by the AFM image. Due to the determined morphology of the perovskite, the small molecular size of the HTM material and its amorphous state in the film phase increase the contact points at the perovskite/HTM interface and initiate charge transfer at the interface [28]. The absorption spectrum of the perovskite film is in the range of 300-750 nm (Figure 4.). In other words, it covers almost the entire visible region. In addition, the absorption band of P3HT in the solution (chlorobenzene) phase is in the range of 300-550nm (λ_{max}=453nm) and that of Spiro-O-MeTAD is in the range of 360-420nm (λ_{max}=389nm).
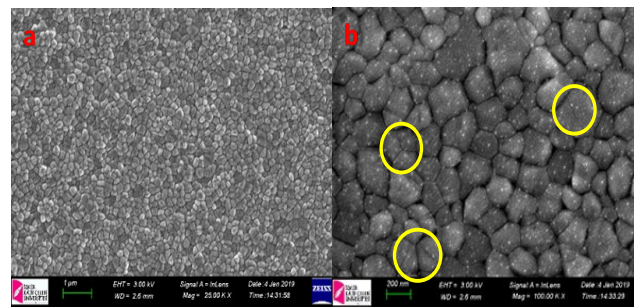
Figure 3. (a) 25kX and (b) 100kX SEM images of triple cation perovskite thin film.
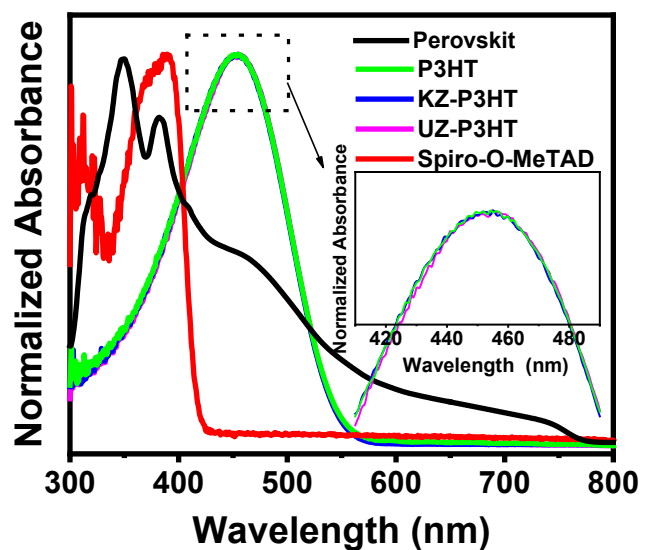
Figure 4. Absorption spectra of perovskit and HTM materials.

B. Gültekin

Figure 5. AFM images of different HTLs. Here (a) 50µm and (b) 5µm Spiro-O-MeTAD, (c) 50µm and (d) 5µm P3HT, (e) 50µm and (f) 5µm UZ- P3HT, (g) 50 µm and (h) 5 µm UZ-P3HT nanowire, (i) 50 µm and (j) 5 µm KZ-P3HT, (k) 50µm and (l) 5µm KZ-P3HT nanowire.

Separation of P3HT into low and high molecular weights did not cause differences in the maximum wavelengths (λ_{max}) in the absorption spectra. This is an expected situation. Because after the critical chain length is exceeded, the optical properties of semiconductor polymers do not show any change in the solution phase in the absence of any stereochemical differences (such as regioregular-regiorandom). This is because the resulting physical properties become ineffective as the chain length increases, as the intermolecular interactions in the solution phase are almost non-existent. However, in the solid phase, since the chain length change of the polymers leads to

changes in the morphology of the thin films, it also directly affects the charge transfer processes. Thin-film morphology directly influences charge transport and interfacial charge transfer processes [24].

The structural properties and stereochemistry of the molecules used in the HTM layer are also factors that directly affect the morphology of the film. For these reasons, film morphologies were investigated by AFM analysis in order to determine the physical changes that appeared by the changes in the polymer chain length. In Figure 5, AFM images of bare P3HT, long-chain P3HT (UZ-P3HT) and short-chain P3HT (KZ-P3HT) films coated on perovskite layer are presented together with

that of Spiro-O-MeTAD. As can be understood from the AFM images, it is observed that the HTMs are in an amorphous structure. However, it can be claimed that nanowires have a more regular morphology. After the P3HT polymer is dissolved in its solvent (chlorobenzene), a weak solvent (hexane) is added to it. The weak solvent interacts with the alkyl chains of P3HT after the addition, reducing the vibrational motion of the chains and allowing π-orbitals of neighbouring polymers to overlap with its own π-orbitals. After that, π-π stacking takes place along the entire chain and forms the nanowire structure [24].

Table 1 Morphology properties of HTM thin films.

HTL	RMS roughness (nm)	Avarage height (nm)	Areal Avarage roughness (nm)
Spiro-O-MeTAD	8.09	59.91	6.60
P3HT	10.62	79.77	8.50
KZ-P3HT	57.35	541.88	42.99
KZ-P3HT Nano wire	13.64	126.89	10.74
UZ-P3HT	72.60	222.20	64.20
UZ-P3HT Nano wire	9.47	74.08	7.62

Although nanowire formation causes a redshift in the absorption spectrum, its more dominant effect in device applications is due to the film morphology. According to the performance parameters in Table 2, the device with the highest efficiency is Spiro-O-MeTAD. However, no doping was applied to he P3HT layers and an efficiency of 5.99% was obtained. In the literature, it has been stated that relatively higher efficiency is obtained from the devices for polymeric HTMs when the polydispersity is low and the chain length is high [23]. However, contrary to the literature, in this study, KZ-P3HT with low molecular weight showed higher performance thanks to its morphological features. As seen in Figure 5, the AFM image of KZ-P3HT is distinctly different from other images with the nano-spots on it, while it is almost the same for all other films obtained with P3HT in 50µm images. In the 5µm images taken for further examination, it is observed that the KZ-P3HT chains form films in heaps, and also, due to the short-chain size, the ends of some chains are seen to protrude out of the stacks and form fringes. It is possible for this structure to improve the perovskite/HTM interface by penetrating into the crystal defects on the perovskite surface like the Spiro-O-MeTAD structure. Thus, the charge transfer increases and also the short-circuit currents obtained from the device containing the KZ-P3HT HTM increase (Table 2).
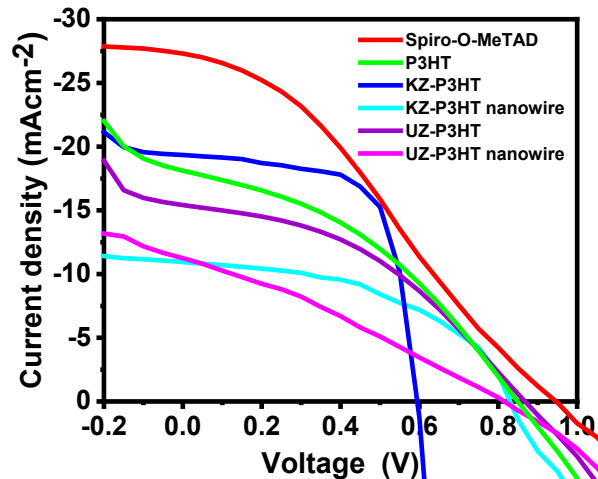
Figure 6. I-V curves of PSC devices with various HTM materials.

In order to examine the morphology of the films coated with nanowires of UZ-P3HT and KZ-P3HT polymers, 5µm and 50 µm AFM images were taken. It is observed that narrower peaks are formed as a result of the transformation of the UZ-P3HT structure into nanowires. Looking at the 5 µm images, it is seen that the islets on the surface of the UZ-P3HT film have turned into smaller and more prominent indentations and protrusions, while the RMS roughness has decreased (Table 1). It is thought that the increase in the short-circuit current and filling factor in the devices produced with UZ-P3HT nanowires is due to the mentioned changes in the nanowire morphology. While the nanowires forming the HTM layer increase the amount of contact at the perovskite-HTM interface, on the other hand, the charge transport within the HTM layer increases thanks to the nano-wire structure [24]. The same situation could not be observed in the transition of KZ-P3HT to the nanowire structure. As seen from the AFM images, because of KZ-P3HT's transition to the nanowire structure, the fringed structures on the film disappeared and the morphology became completely the same as the other P3HT structures. As a result, device efficiency has decreased to the level of device efficiency based on P3HT and UZ-P3HT.

PV performance tests were carried out under AM 1.5 G, with the devices created as specified in the device fabrication section. Before the PV performance analysis, the light intensity of the simulator was calibrated with a silicon solar cell with an area of 4 cm^2. The resulting J-V graphs are exhibited in Figure 6 and the performance parameters are summarized in Table 2. Among the devices prepared after annealing the perovskite active layer at 100 ºC, a power conversion efficiency of 8.69% was obtained with the standard Spiro-O-MeTAD, while a power conversion efficiency of 5.99% was obtained with the standard P3HT.

When the PV performances of UZ and KZ P3HT based devices are evaluated, it is noticed that KZ-P3HT exhibits higher power conversion efficiency (PCE) (7.74%) than P3HT. As indicated in the AFM results, in contrast to P3HT and UZ-P3HT, the fringed structure of KZ-P3HT in the film phase increases the contact points at the perovskite/HTM interface, thereby reducing trap levels.

Table 2. PV performances of PSC devices with various HTMs.

HTL	$J_{SC(MAX)}$ (mA cm^{-2})	V_{OC} (MAX) (mV)	FF (MAX)	PCE (MAX) (%)
Spiro-OMeTAD	27.51	950	0.33	8.69
P3HT	18.11	850	0.39	5.99
KZ-P3HT	19.35	650	0.66	7.74
KZ-P3HT Nanowire	10.94	820	0.62	5.81
UZ-P3HT	10.70	800	0.31	2.68
UZ-P3HT Nanowire	15.42	870	0.42	5.51

The relatively higher fill factor (FF) and short-circuit current (I_{SC}) observed in electrical measurements are proof of this result. On the other hand, the PCE of the device in which UZ-P3HT is used as HTM is far below P3HT. The main reasons for the 2.68% efficiency obtained from the KZ-P3HT are its low short-circuit current (I_{SC}) and fill factor (FF). This result shows that electron-hole pairs (exciton) formed in the perovskite layer are highly recombined (recombined) without dissociation at the perovskite/HTM interface. If we look at the PSC applications of nanowire structures of UZ and KZ P3HTs, it is seen that both structures present PCE values close to each other. As observed in the AFM images, both nanowire thin films have the same morphologies. In this case, due to the decrease in the contact points of the KZ-P3HT nanowire at the perovskite/HTM interface, a significant decrease in I_{SC} occurred.

4. Conclusion

As a result, the effects of chain length-dependent morphology changes of P3HT, which is used as an alternative to Spiro-O-MeTAD in PSC devices, on PCE were determined comparatively. The PCEs of Spiro-O-MeTAD and P3HT-based devices were 8.69% and 5.99%, respectively, while the PCEs of KZ-P3HT and UZ-P3HT-based devices were 7.74% and 2.68%, respectively. In particular, it is thought that the fringed structure of KZ-P3HT, determined by AFM images, increases the amount of contact by penetrating the boundaries between the crystal particles observed on the perovskite surface, thus improving the perovskite/HTM

interface. Thus, it is understood from the increase of I_{SC} in the J-V characteristic of the device that higher charge transfer is provided than the standard P3HT. In addition, the effects of P3HT nanowire structures on device performances were also revealed through morphology and interface properties. In devices prepared with nanowires of UZ-P3HT, PCE increased from 2.68% to 5.51%. This is thought to be due to the increased charge transfer on the HTM layer via more ordered aggregation of the P3HT chains. In particular, the increase in I_{SC} and FF values indicates an increase in charge transfer. Contrary to UZ-P3HT nanowires, the efficiency of devices containing KZ-P3HT nanowires decreased by 5.81%. In AFM images, it was observed that the fringed structure of KZ-P3HT disappeared after conversion to nanowire. For this reason, it was concluded that the interfacial interactions decreased and thus the efficiency decreased.

Acknowledgement

Author's Contributions

Oğuz Çiçek: Performed the experiments and result analyses, drafted the manuscript.
Burak Gültekin: Supervised and managed the study, drafted, and wrote the manuscript.

Ethics

There are no ethical issues after the publication of this manuscript.

References

[1]. "Best Research-Cell Efficiency Chart | Photovoltaic Research | NREL." https://www.nrel.gov/pv/cell-efficiency.html (accessed Dec.. 3, 2021).

[2]. M. Saliba *et al.*, 2016, "Cesium-containing triple cation perovskite solar cells: Improved stability, reproducibility and high efficiency," *Energy and Environmental Science*, 9(6), 1989–1997.

[3]. M. Liu, M. B. Johnston, and H. J. Snaith, 2013, "Efficient planar heterojunction perovskite solar cells by vapour deposition," *Nature*, 501(7467): 395–398.

[4]. O. Almora *et al.*, 2021, "Device Performance of Emerging Photovoltaic Materials (Version 1)," *Advanced Energy Materials*, 11(11).

[5]. S. S. Ashrafi *et al.*, 2020, "Characterization and Fabrication of Pb-Based Perovskites Solar Cells under Atmospheric Condition and Stability Enhancement," *Advances in Materials Physics and Chemistry*, 10(11): 282–296.

[6]. Q. Chen *et al.*, 2014, "Planar Heterojunction Perovskite Solar Cells via Vapor-Assisted Solution Process,", *Journal of the American*

Chemical Society, 136(2): 3–6.

[7]. G. E. Eperon, V. M. Burlakov, P. Docampo, A. Goriely, and H. J. Snaith, 2014, **"**Morphological Control for High Performance , Solution- Processed Planar Heterojunction Perovskite Solar Cells,", Advanced Functional Materials, 24 (1): 151–157.

[8]. S. Rutile *et al.*, 2013, **"**High Efficiency Solid-State Sensitized Solar Cell-Based on Submicrometer Rutile TiO 2 Nanorod and CH 3 NH 3 PbI 3 Perovskite Sensitizer", *Nano Letters,* 13(6): 2412-2417.

[9]. K. Wojciechowski, M. Saliba, T. Leijtens, A. Abate, and H. J. Snaith, 2014, "Environmental Science Sub-150 C processed meso-superstructured perovskite solar cells with enhanced efficiency", *Energy and Environmental Science*, 7(3), 1142–1147.

[10]. Q. An, P. Fassl, Y. J. Hofstetter, D. Becker-koch, and A. Bausch, 2017, "Nano Energy High performance planar perovskite solar cells by ZnO electron transport layer engineering", *Nano Energy*, 39(4): 400–408.

[11]. T. Matsui, W. Tress, M. Saliba, A. Abate, M. Gra, and A. Hagfeldt, 2016, "Environmental Science cells by solution-processed tin oxide", *Energy & Environmental Science*, 9: 3128–3134.

[12]. Y. Wu *et al.*, 2016, "Perovskite solar cells with 18.21% efficiency and area over 1 cm2 fabricated by heterojunction engineering", *Nature Energy,* 1(11):1–7.

[13]. P. Yadav, D. Prochowicz, M. Saliba, P. P. Boix, S. M. Zakeeruddin, and M. Grätzel, 2017, "Interfacial kinetics of efficient perovskite solar cells,**"** *Crystals*, 7(8)**:**1–9.

[14]. L. Miao, Z. Song, D. Zhu, L. Li, L. Gan, and M. Liu, 2020, "Recent advances in carbon-based supercapacitors," *Materials Advances*, 1(5):945–966.

[15]. T. Leijtens, K. Bush, R. Cheacharoen, R. Beal, A. Bowring, and M. D. McGehee, 2017, "Towards enabling stable lead halide perovskite solar cells," *J. Mater. Chem. A*, 5(23), 11483–11500.

[16]. M. Kim *et al.*, 2021, "Moisture resistance in perovskite solar cells attributed to a water-splitting layer," *Communications Materials 2021 2:1*, 2(1), 1–12.

[17]. G. Ren *et al.*, 2021, "Strategies of modifying spiro-OMeTAD materials for perovskite solar cells: a review," *Journal of Materials Chemistry A*, 9(8): 4589–4625.

[18]. J. Y. Seo *et al.*, 2021, "Dopant Engineering for Spiro-OMeTAD Hole-Transporting Materials towards Efficient Perovskite Solar Cells," *Advanced Functional Materials*, 31(45): 2102124.

[19]. X. Sun, X. Yu, and Z. Li, 2020, "Recent advances of dopant-free polymer hole-transporting materials for perovskite solar cells," *ACS Applied Energy Materials*, 3(11)**:** 10282–10302.

[20]. N. Yaghoobi Nia *et al.*, 2021, "Impact of P3HT Regioregularity and Molecular Weight on the Efficiency and Stability of Perovskite Solar Cells," *ACS Sustainable Chemistry and Engineering*, 9(14): 5061–5073.

[21]. Y. Zhang, M. Elawad, Z. Yu, X. Jiang, J. Lai, and L. Sun, 2016, "Enhanced performance of perovskite solar cells with P3HT hole-transporting materials via molecular p-type doping," *RSC Advances*, 6(110): 108888–108895.

[22]. E. H. Jung *et al.*, 2019, "Efficient, stable and scalable perovskite solar cells using poly(3-hexylthiophene)," *Nature 2019 567:7749*, 567(7749): 511–515.

[23]. N. Y. Nia, F. Matteocci, L. Cina, and A. Di Carlo, 2017, "High-Efficiency Perovskite Solar Cell Based on Poly(3-Hexylthiophene): Influence of Molecular Weight and Mesoscopic Scaffold Layer," *ChemSusChem*, 10(19): 3854–3860.

[24]. D. Kiymaz, A. Kiymaz, and C. Zafer, 2020, **"**Performance improvement of P3HT nanowire-based organic solar cells by interfacial morphology engineering,**"** *Nanotechnology*: 32(10)**,** 105401.

[25]. N. Y. Nia, F. Matteocci, L. Cina, and A. Di, 2017, "High-Efficiency Perovskite Solar Cell Based on Poly (3-Hexylthiophene): Influence of Molecular Weight and Mesoscopic Scaffold Layer," *Aldo Di Carlo*, 10 (19) : 3854–3860.

[26]. M. Sapolsky and D. Boucher, 2018, "Poly (3-Hexylthiophene) Aggregation at Solvent – Solvent Interfaces,**"** *Journal of Polymer Science, Part B: Polymer Physics***,** 56 (13): 999–1011.

[27]. Y. Wang *et al.*, 2017, "Stitching triple cation perovskite by a mixed anti-solvent process for high performance perovskite solar cells," *Nano Energy*, 39(July): 616–625.

[28]. J. W. Lee, S. H. Bae, N. De Marco, Y. T. Hsieh, Z. Dai, and Y. Yang, 2018, "The role of grain boundaries in perovskite solar cells,**"** *Materials Today Energy***,** 7**:** 149–160.

[29]. L. Tian *et al.*, 2020, "Effects of Annealing Time on Triple Cation Perovskite Films and Their Solar Cells," *ACS Applied Materials and Interfaces*, 12(26): 29344–29356.